Influence of pumping/extrusion on the air-void system of 3D printed concrete

Author(s):
Das, Arnesh; Song, Yu; Mantellato, Sara; Wangler, Timothy; Flatt, Robert J.; Lange, David

Publication date:
2020-07

Permanent link:
https://doi.org/https://doi.org/10.3929/ethz-b-000426811

Originally published in:
RILEM Bookseries 28

Influence of Pumping/Extrusion on the Air-void System of 3D Printed Concrete

Arnesh Das[1], Yu Song[2,3], Sara Mantellato[1], Timothy Wangler[1], Robert J. Flatt[1], David A. Lange[2]

[1]Institute for Building Materials, ETH Zurich, Zurich, Switzerland
[2]Department of Civil and Environmental Engineering, University of Illinois Urbana-Champaign, IL, USA
[3]Physics of AmoRphous and Inorganic Solids Laboratory (PARIS lab), Department of Civil and Environmental Engineering, University of California, Los Angeles, CA, USA

Abstract
3D printing with concrete offers many advantages over conventional construction methods and interest in this field of research has seen a rapid rise in recent years. While there have been large number of cases of successful fabrication of 3D printed structures, ensuring the long-term durability performance of the fabricated structures is equally important. Freeze-thaw damage is one such deterioration issue, especially in cold places like Switzerland. This study investigated the effect of the different processing conditions encountered in 3D printing, namely pumping, acceleration/mixing and extrusion on the air void system of a standard 3D printable mortar mix. The 3D void size distribution of the air voids obtained using a recently developed stereological model, along with the ASTM C457 results showed that pumping had the major impact on the void structure as both air content and spacing factor decreased significantly. The effect of acceleration/change in rheology and extrusion on the void structure was also prominent from the obtained results. The 3D protected paste volume (PPV) curves showed that pumping and acceleration processes could enhance the freeze-thaw performance.

Keywords: 3D printing, freeze-thaw, pumping, extrusion, PPV.

1. Introduction

Concrete research has been reshaped in recent years due to a host of emerging digital fabrication techniques, with 3D concrete printing/layered extrusion being the most extensively researched topic [1–3]. Compared to the conventional construction methods, this new approach offers numerous advantages in terms of cost, time, constructability and workspace safety [4]. 3D printing is a process whereby the fresh material is extruded through a mobile nozzle but, once printed, the material should support its self-weight as well as the layers placed further above. As such, an ideal printable concrete material is expected to be initially flowable between mixing and pumping (open time), next placeable with certain shape-holding ability during printing, and then strong enough to sustain weight applied by subsequently deposited material [5]. One common way to achieve this is by the appropriate usage of chemical admixtures [6], particularly for structures with high vertical building rate. In such cases, the hydration of cement is initially retarded but then also accelerated just before the extrusion process. Such process can generically be defined as setting on demand [7]

To date, there have been a large number of successful cases of 3D fabricated structures. Engineering wise, however, the long-term durability performance of these structures deserves more attention. One pertinent issue is the freeze-thaw damage of concrete, which is especially critical in cold places like Switzerland. To cope with this problem, air-entraining admixtures have been long added into fresh concrete for enhancing the frost resistance. Experience has shown that the air content measured in the fresh state alone does not define a concrete's freeze-thaw resistance, but that this can be assessed from the spacing factor between air voids in hardened concrete [8,9]. According to Powers, the concept of spacing factor assumes that voids are mono sized spheres which are uniformly distributed in the cement paste with a cubic lattice network [10]. For good freeze-thaw resistance, the spacing factor value should be less than 200 μm, while for high-strength concrete, it could be up to 250 μm [11,12]. ASTM C457 describes a microscope-based method for estimating the various hardened air-void parameters [13]. However, this test is cumbersome as it involves very time-consuming repeated visual determination of the concrete material phases-aggregates, cement paste and the air voids. Another limitation of the ASTM method is that measurements are only one/two dimensional, while air void distribution is a three-dimensional concept in reality. To overcome these limitations, researchers have developed various techniques to facilitate the testing, with the flatbed scanner method being the most widely accepted [14–17].

With regard to hardened air void analysis for assessing frost resistance of concrete, the literature mentions studies about protected paste volume (PPV) [14,18]. The PPV concept is linked to the original idea of the spacing factor and this analysis goes by the assumption that an air void has a protecting influence on cement paste (over a certain assigned range) from freeze-thaw damage. The previous practice has been to carry out this analysis on 2D polished sections of concrete and this quantifies the degree of protection by computing the fraction of paste falling into the

protection range on a 2D plane [19]. However, such a 2D PPV analysis has certain limitations. The radius of an air void on an inspected surface appearing on the section tends to be smaller than the actual radius of the void, hence the protection range around an intersected air void (referred to as in-section void) would vary depending on the cut position. Also, certain sections of the inspected concrete surface may be protected by an un-intersected air void (referred to as out-section void). Thus, the 2D PPV analysis underestimates the protected range and in order to accurately estimate the degree of protection, the 3D distribution of both in and out-section voids must be determined [20]. This can be done by a stereological model recently developed by Song et al. [20]. The results obtained by this model have been found to align well with those obtained by other authors using techniques such as numerical simulation and computed tomography. Fig. 1 illustrates the difference between the 2D PPV analysis and the actual protected zone [20]. In the figure, the in-section voids are shown in blue, the out-section voids in orange and the protected paste in green.

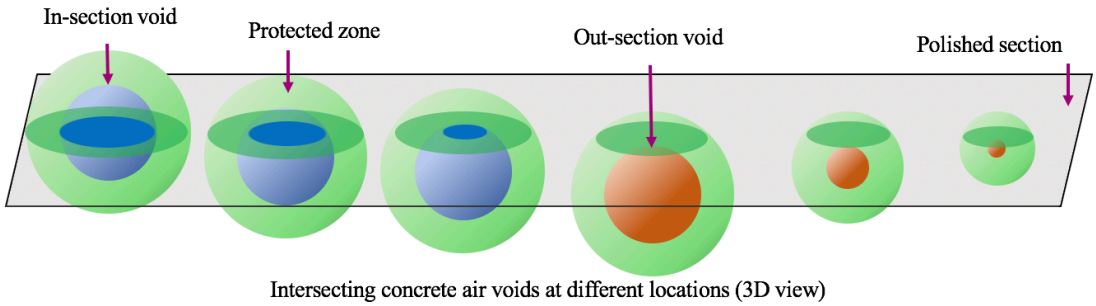

Fig. 1. Difference between 2D PPV analysis and the actual protected zone. Permission requested from [20].

Previous studies have shown that the air void system of concrete can be readily altered by the placement method during the fresh stage. This issue can be more pronounced in case of 3D printable concrete, as both pumping and extrusion can impose a greater influence than normal concrete placement methods. The potential interaction between the different chemical admixtures further complicates the situation. In this paper, the impact of the different processing conditions encountered in 3D printing, namely pumping, acceleration/mixing and extrusion on the air void system is studied. The hardened air void analysis is carried out on a standard 3D printable mortar mix after the various processing steps.

2. Materials and Methods

2.1 Material

This study was carried out based on samples cast from a single batch of mortar mix, with the different processing conditions. The batch mix consisted of crushed limestone aggregates (maximum size of 2 mm; 46% by volume), CEM I 52.5R (Holcim Normo 5R) cement, silica fume and limestone filler (8% and 15% by weight of cementitious material respectively). PCE based superplasticizer BASF MasterGlenium ACE30 (Switzerland) and 30% sucrose solution were used (1% and 0.2% by weight of cementitious material respectively). A calcium aluminate cement (CAC; Ciment Fondu, source: Kerneos) paste retarded with 0.1% sodium gluconate was used as the accelerator. The water to cement ratio for both the retarded base mortar mix and CAC paste were 0.38. After being pumped, the mortar mix was mixed with the CAC paste accelerator at the nozzle. The flow rate for the mortar mix was 1.4 L/min, while that for the accelerator mix was 54 mL/min and the residence time at the mixing chamber was 30 seconds. The pumping and extrusion pressures were 1.2 bar and 0.2 bar respectively. The material was collected after the different processing steps and cast into Plexiglas cylindrical molds having diameter of 9 cm and height of 12 cm, to create four different groups: Group A (Base mix retarded before pumping); Group B (Base mix retarded after pumping); Group C (Base mix extruded, but not accelerated) and Group D (Base mix accelerated and extruded). The idea behind creating these groups of mixes was to see if the change in rheology after acceleration also has an effect on the air void system, in addition to the pumping and extrusion. One cylinder was cast (with compaction to get rid of most of the entrapped air) for each group and these were all cured in a chamber with 95% relative humidity for at least 14 days, before being worked upon.

2.2 Sample preparation/scanning and image segmentation/processing

The cylinder samples were first saw-cut along their axis into two half cylinders which were further saw-cut into half to yield four half cylinders of 9 cm by 6 cm. These samples were then polished according to the method

specified in ASTM C457 [13]. The method of sample preparation/scanning was similar to that followed by Song et al. [17].

After the polishing step, it was ensured that the surface was dried. An orange fluorescent chalk powder (Irwin Marking Chalk) was used to fill the air voids. Once all the air voids were filled, the excess powder was struck off by running a sharp razor blade over the surface at a very low angle. Care was taken not to scratch the surface during this step. All samples were then scanned with a commercial-grade flatbed scanner (CanoScan5600F) with a resolution of 4800 dpi (edge length of each pixel being 5.3 μm). In order to satisfy the minimum scanned area of 75 cm^2, as specified in ASTM C457 [13], three samples from each group were worked upon and the size of each scan was 5 cm by 5 cm. After obtaining the scan, the next step was image segmentation. This was done using a deep learning neural network (NN) model. During the final processing, air voids smaller than 10 μm and aggregates smaller than 100 μm were removed as a noise reduction step. The pores present in the aggregates were also filled and finally, a ternary image showing the different phases was yielded. Eventually, an automated analysis was conducted to compute the various ASTM C457 parameters from the ternary images.

2.3 3D analysis

For the computation of the various 3D parameters, a convolutional neural network (CNN) model was used. More details about the CNN model can be found in literature [21]. This model was developed based on the state-of-the-art CNN DeepLabv3 [22] and ResNet-101 [23] and has shown remarkable performance [24,25]. PyTorch, which is an open-source machine learning library in Python was used for implementing the algorithm. The following 3D parameters were computed using the model:

- 3D void model: This shows the 3D distribution of the in and out-section voids. The out-section voids are the un-intersected voids whose protection range falls on the inspected section. These are estimated from the actual void size distribution of the in-section voids and an assumed protection range. The protection range was taken as 200 μm. The 3D protection yield (PPV map) from all voids were also obtained.

- 3D void size distribution of in-section voids: This refers to the actual void size distribution of the intersected voids. These are estimated from the 2D or apparent void size distribution of the voids on the inspected section.

- 3D paste protection: This quantifies the degree of 3D paste protected as a function of the assumed protection range. This is done based on the same principle as PPV concept.

3. Results and Discussion

A typical scan and its processed ternary image are shown in Fig. 2 (a). Fig. 2 (b) shows the magnified versions (image section being 1.7 cm by 1.7 cm) of the top right corner of the images. This example represents the general quality of the original scans and the segmented images done by the CNN model. The processed ternary image was then used to compute the various ASTM C457 parameters and the 3D air void results.

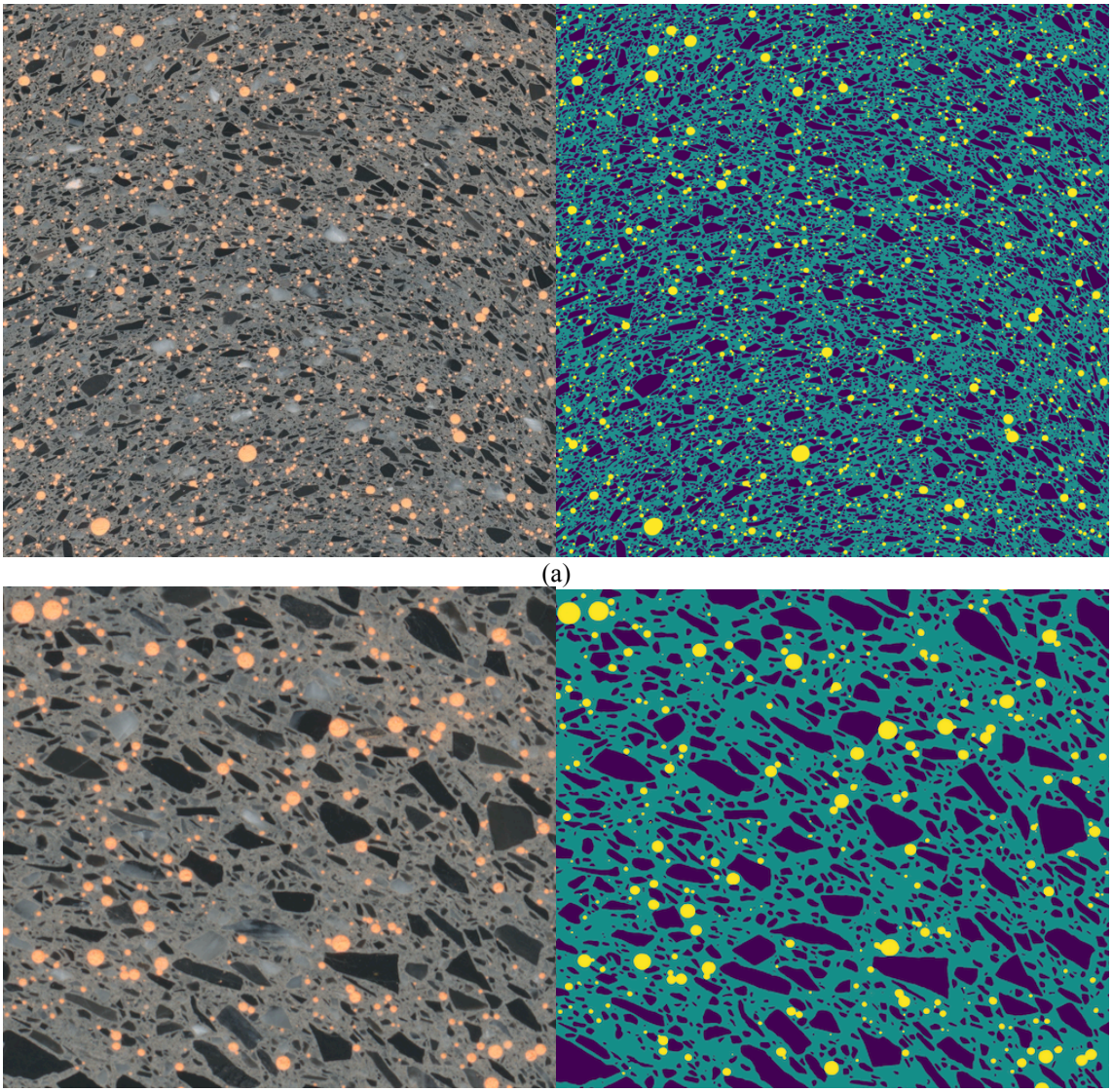

Fig. 2. (a) Original scan and its processed ternary image of sample D1 (5 cm by 5 cm); (b) magnified versions of the top right corner of the images (1.7 cm by 1.7 cm)

Based on the segmented images, the aggregate content, paste content, air content and spacing factor of the different groups of samples are shown in Table 1. The mortar mix is not freeze-thaw resistant as the spacing factor values are higher than the prescribed 200 μm [13]. The results also confirm that the pumping action does alter the void structure as both air content and spacing factor decrease. However, the difference in spacing factor values between Groups B, C and D is neglectable. The difference in air content values between them could be due to some entrapped air formed during the casting process.

Table 1. Air void parameters of the different groups of samples for three independent scanned areas of 25 cm^2 each

Group	Aggregate content [%]	Paste content [%]	Air content [%]	Spacing factor [μm]
A	38.7 ± 0.4	57.2 ± 0.9	4.2 ± 0.5	529 ± 15
B	37.7 ± 0.4	59.0 ± 0.4	3.3 ± 0.1	436 ± 1
C	38.8 ± 0.5	57.5 ± 0.4	3.8 ± 0.6	458 ± 14
D	36.1 ± 0.1	59.9 ± 0.1	4.0 ± 0.1	441 ± 20

Fig. 3 (a) shows the 3D void model of the top right corner of sample D1 (section size of 1.7 cm by 1.7 cm), as an example. In this figure, the blue spheres denote the in-section voids, while the out-section voids are represented by the yellow spheres. The semi-transparent shells around them indicate the assumed protection range. It is to be noted that the assumed protection range of 200 μm is an arbitrary value, which has often been taken in literature

for analysis and this does not imply any real physical protection range as there is no evidence yet, to confirm this. Fig. 3 (b) shows the protected paste volume (PPV) map, which is available as partial size corresponding to the partial 3D model displayed in Fig. 3 (a). The 3D PPV map illustrates the spatial information of the various phases. In the figure, the color annotation has been done in a way to better qualify the protection degree as function of the assumed protection range. The protected paste in the figure makes a transition from green to yellow while the red zone (for protection range above 300 μm) indicates the unprotected paste.

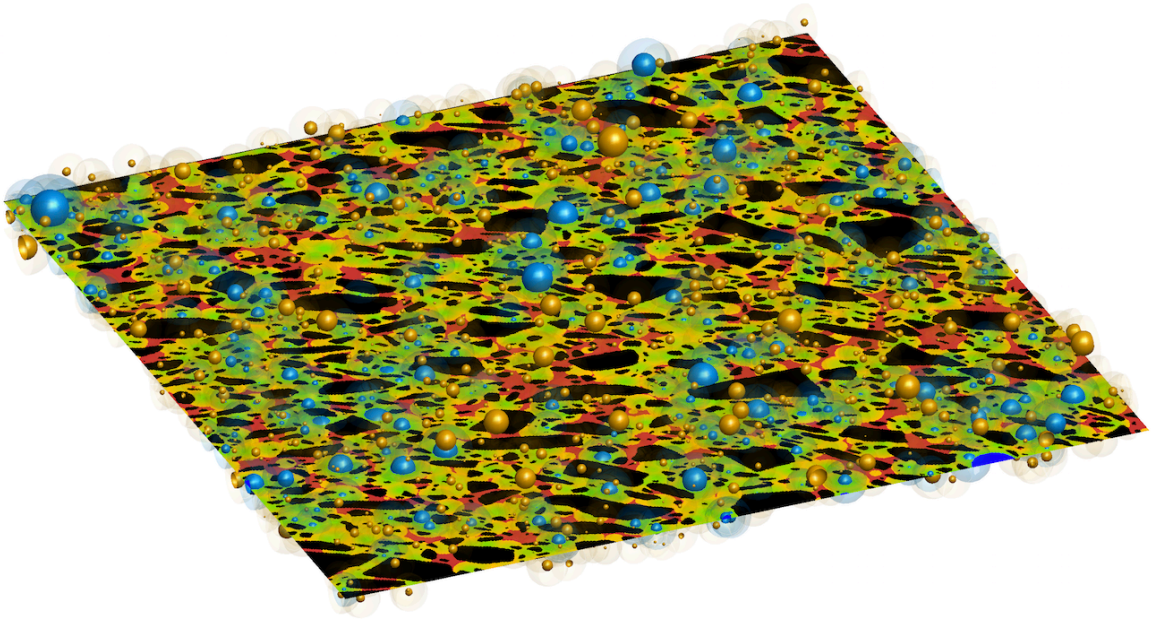

(a)

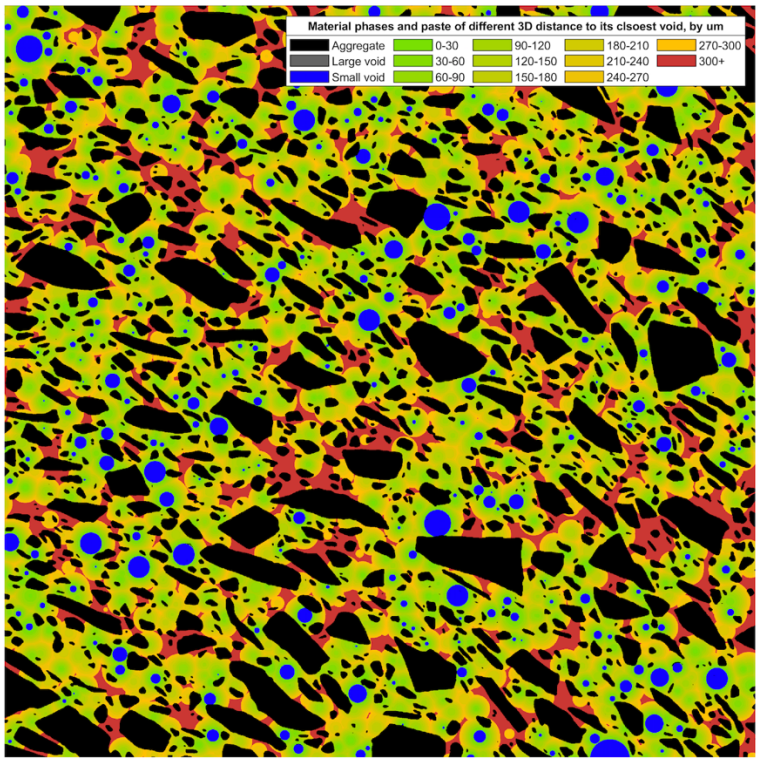

(b)

Fig. 3. (a) 3D void model of top right corner of sample D1; (b) partial PPV map of sample D1 corresponding to partial model displayed in (a)

Fig. 4. shows the 3D void size distribution (VSD) of the samples from every group along with their error bars. The VSD curves show decent consistency within the same group and contrast can be seen between the different groups. Comparing Groups A and B, it is seen that the pumping breaks the 'oversized' air voids (> 300 μm) into smaller ones such that a larger concentration of smaller voids (< 100 μm) per unit volume is seen after the pumping. This could explain the decrease in spacing factor between Groups A and B. There is also some loss of air as can be seen by the decrease in air content. The fact that pumping can alter the void structure has also been found by other researchers [26,27]. A different observation was reported by Pleau et. al, 1995 [27]. They found that pumping removes the 'smaller' air voids but the larger ones are little affected. However, it is important to note that their pumping pressures were much higher, of the order of 15-30 bar, in contrast to the 1.2 bar used for the current study. It is likely that in addition to the pumping pressures, the actual impact of pumping on the air void system would also depend on other factors such as mix design/rheological properties of the mix and how well air-entrained the mix is.

Although the ASTM C457 results illustrated in Table 1 show that the spacing factor did not change significantly between Groups B, C and D, a notable change is found regarding the VSD curves. In particular, the curve for Group C tends to shift rightwards. Hence, both the acceleration and extrusion (even at a pressure as low as 0.2 bar) can change the void structure. The difference in the VSD curves of Groups C and D indicates the effect of rheology on the air void system of the extruded material.

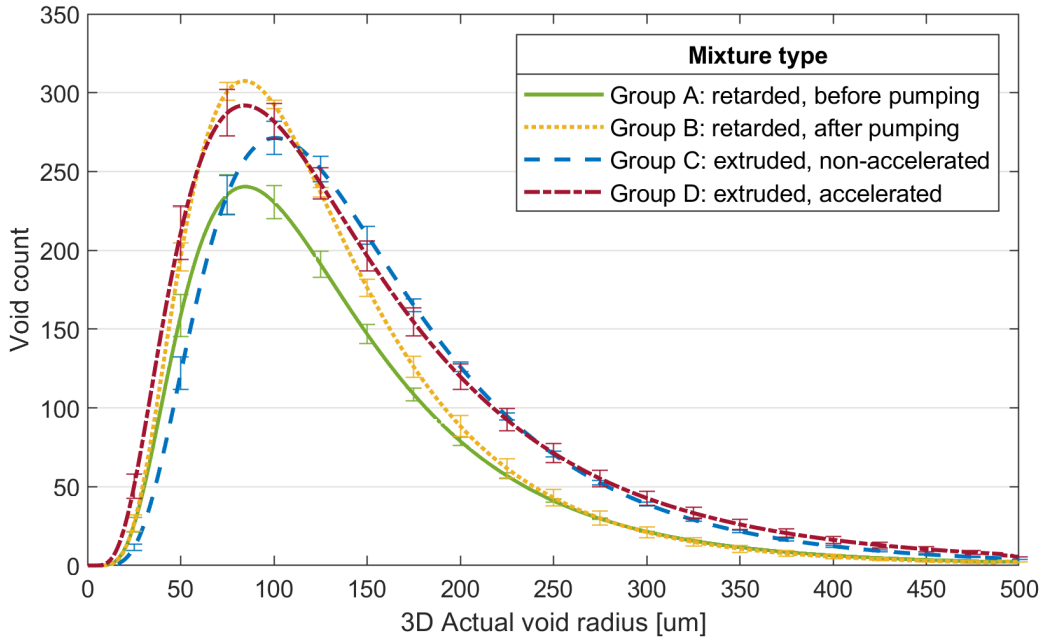

Fig. 4. Void Size Distribution (VSD) curves for different groups of samples

The degree of protection of a concrete mixture from freeze-thaw damage depends on the assumed value of protection range. Fig. 5. shows the degree of 3D protection for the different groups as a function of the assumed protection range. It can be seen that the degree of protection increases non-linearly as the protection range increases. The difference in the degrees of protection between the different groups of samples can also be seen. Group C, in particular is less protected compared to the other groups. This observation also aligns well with the 3D VSD results where it is seen that Group C has a relatively higher concentration of voids larger than 100 μm. This also supports the notion that a higher concentration of closely spaced 'smaller' sized air bubbles is good for freeze-thaw protection.

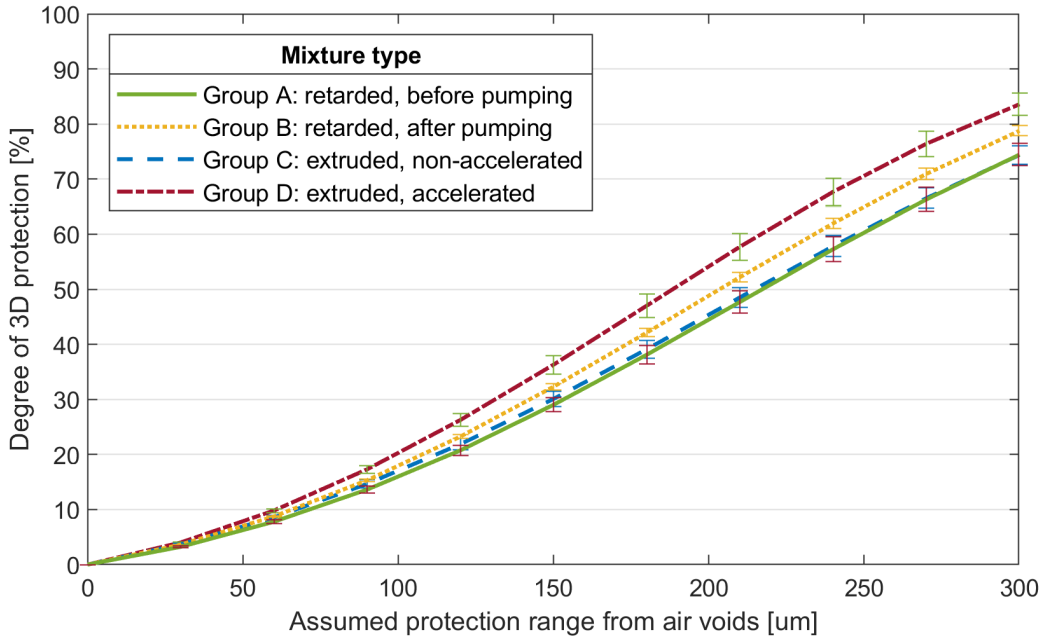

Fig. 5. Degree of 3D protection as function of assumed protection range for the different groups

Group B has a higher concentration of smaller sized air voids (< 100 μm) and a smaller spacing factor compared to Group A, hence, if the mix was well air-entrained, the pumping action could possibly enhance its freeze-thaw performance. Pertaining to the requirements of 3D printing, an acceleration of cement hydration is most often necessary before the extrusion process. This also augurs well for the freeze-thaw performance as can be seen from the 3D PPV curves of Groups C and D. In short, provided the base mix is well designed in terms of freeze-thaw resistance, 3D extrusion should not compromise that property either because of processing or use of accelerators. Until such conclusions are more broadly validated, it is however recommended to test the air void spacing of 3D printed concrete that will be exposed to freeze-thaw cycles. The methods used in this paper offer a way of doing so.

As a next step in this work, the same analyses will be carried out on a 3D printable mortar mix with different levels of air-entrainment. While it is expected that air-entraining admixtures (AEAs) will lead to a more stable air-void system, it will be interesting to assess the effect of the different processing conditions on such a system. The potential interaction between the defoamers present in superplasticizers and the AEAs can possibly further affect the stability.

4. Conclusions

3D printing with concrete most often involves the following processing steps: pumping; acceleration/mixing; and extrusion. In this study, the effect of these processing conditions on the air void system of a 3D printable mortar mix was studied. The analyses was done based on the ASTM C457 results as well as 3D VSD and 3D PPV curves. It was found that pumping had the most severe impact on the air void system as both air content and spacing factor decreased significantly. The effect of acceleration/change in rheology and extrusion on the void structure was also prominent from the obtained results. In particular, Group C showed a relatively higher concentration of air voids larger than 100 μm, and it was found to be less well protected from freeze-thaw damage compared to other groups. If the mortar mix is well air-entrained, then the implications of the pumping and acceleration on the freeze-thaw performance are evident from the results.

Acknowledgements

This research was supported by the NCCR Digital Fabrication, funded by the Swiss National Science Foundation. (NCCR Digital Fabrication, Agreement # 51NF40-141853). The authors would also like to thank Dr. Lex Reiter (PCBM group, ETH Zurich) for the useful discussions and for his support during this work and also acknowledge Heinz Richner (PCBM group, ETH Zurich) for the help in saw-cutting the hardened concrete samples.

References

1. Buswell RA, Leal de Silva WR, Jones SZ, Dirrenberger J. 3D printing using concrete extrusion: A roadmap for research. *Cem Concr Res*. 2018;112:37-49. doi:10.1016/j.cemconres.2018.05.006

2. Khoshnevis B. Automated construction by contour crafting—related robotics and information technologies. *Autom Constr*. 2004;13(1):5-19. doi:10.1016/j.autcon.2003.08.012

3. Roussel N. Rheological requirements for printable concretes. *Cem Concr Res*. 2018;112:76-85. doi:10.1016/j.cemconres.2018.04.005

4. Reiter L, Wangler T, Roussel N, Flatt RJ. The role of early age structural build-up in digital fabrication with concrete. *Cem Concr Res*. 2018;112:86-95. doi:10.1016/j.cemconres.2018.05.011

5. Wangler T, Lloret E, Reiter L, et al. Digital Concrete: Opportunities and Challenges. *RILEM Tech Lett*. 2016;1:67-75. doi:10.21809/rilemtechlett.2016.16

6. Marchon D, Kawashima S, Bessaies-Bey H, Mantellato S, Ng S. Hydration and rheology control of concrete for digital fabrication: Potential admixtures and cement chemistry. *Cem Concr Res*. 2018;112:96-110. doi:10.1016/j.cemconres.2018.05.014

7. Reiter L, Wangler T, Anton A, Flatt RJ. Setting on demand for digital concrete- principles, measurements, chemistry, validation. *Cem Concr Res*. 2020.

8. Du L, Folliard KJ. Mechanisms of air entrainment in concrete. *Cem Concr Res*. 2005;35(8):1463-1471. doi:10.1016/j.cemconres.2004.07.026

9. Durability of Concrete in Cold Climates | Taylor & Francis Group. https://www.taylorfrancis.com/books/9780429177644. Accessed January 15, 2020.

10. Powers TC. The Air Requirement of Frost-Resistant Concrete. 1949.

11. ACI Committee 212, Report on Chemical Admixtures. 2010.

12. CSA A23.1-14/A23.2-14, CSA A23.1 (Concrete materials and methods of concrete construction) and A23.2 (Test methods and standard practices for concrete). 2014.

13. ASTM C457, Standard Test Method for Microscopical Determination of Parameters of the Air Void System in Hardened Concrete 1. 2013.

14. Peterson KW, Swartz RA, Sutter LL, Van Dam TJ. Hardened Concrete Air Void Analysis with a Flatbed Scanner. *Transp Res Rec*. 2001;1775(1):36-43. doi:10.3141/1775-06

15. Peterson K, Sutter L, Radlinski M. The Practical Application of a Flatbed Scanner for Air-Void Characterization of Hardened Concrete. *Recent Adv Concr Freez-Thawing F-T Durab*. January 2010. doi:10.1520/STP49082S

16. Carlson J, Sutter L, Van Dam T, Peterson KR. Comparison of Flatbed Scanner and RapidAir 457 System for Determining Air Void System Parameters of Hardened Concrete. *Transp Res Rec*. 2006;1979(1):54-59. doi:10.1177/0361198106197900108

17. Song Y, Zou R, Castaneda DI, Riding KA, Lange DA. Advances in Measuring Air-Void Parameters in Hardened Concrete Using a Flatbed Scanner. *J Test Eval*. 2017;45(5):1713-1725. doi:10.1520/JTE20150424

18. Wawrzeńczyk J, Kozak W. Protected Paste Volume (PPV) as a parameter linking the air-pore structure in concrete with the frost resistance results. *Constr Build Mater*. 2016;112:360-365. doi:10.1016/j.conbuildmat.2016.02.196

19. Larson TD, Cady PD, Malloy JJ. THE PROTECTED PASTE VOLUME CONCEPT USING NEW AIR-VOID MEASUREMENT AND DISTRIBUTION TECHNIQUES. *J Mater*. March 1967. https://trid.trb.org/view/101818. Accessed January 15, 2020.

20. Song Y, Damiani RM, Shen C, Castaneda DI, Lange DA. A 3D petrographic analysis for concrete freeze-thaw protection. *Cem Concr Res*. 2020;128:105952. doi:10.1016/j.cemconres.2019.105952

21. Song Y, Huang Z, Shen C, Shi H, Lange DA. Deep learning-based automated image segmentation for concrete petrographic analysis (under review). *Cem Concr Res*. 2020.

22. Chen L-C, Papandreou G, Schroff F, Adam H. Rethinking Atrous Convolution for Semantic Image Segmentation. *ArXiv170605587 Cs*. December 2017. http://arxiv.org/abs/1706.05587. Accessed January 18, 2020.

23. He K, Zhang X, Ren S, Sun J. Deep residual learning for image recognition. 2016.

24. Huang Z, Wang X, Huang L, Huang C, Wei Y, Liu W. CCNet: Criss-Cross Attention for Semantic Segmentation. *ArXiv181111721 Cs*. November 2018. http://arxiv.org/abs/1811.11721. Accessed January 18, 2020.

25. Ruan T, Liu T, Huang Z, et al. Devil in the Details: Towards Accurate Single and Multiple Human Parsing. *ArXiv180905996 Cs*. November 2018. http://arxiv.org/abs/1809.05996. Accessed January 18, 2020.

26. Feys D, Wehar A, Moreno DG, Hutcheson E, Riding KA. How pumping affects the spacing factor of self-consolidating concrete. 2019.

27. Pleau R, Pigeon M, Lamontagne A, Lessard A. Influence of pumping on characteristics of air-void system of high-performance concrete. 1995.